Proceedings of the
Annual Stability Conference
Structural Stability Research Council
Atlanta, Georgia, April 21-24, 2026

Vibration performance of an all-steel floor system using finite element modeling techniques

Rajshri Chidambaram Muthu Kumar[1], Sahabeddin Rifai[2], Abdelrhman Ramadan[3], Onur Avci[4], Matthew Eatherton[5], Benjamin W. Schafer[6]

Abstract

The objective of this research is to investigate the vibration performance of a modular steel floor system using detailed shell finite element modeling, with a focus on the effects of human walking-induced loads. The work is motivated by a proposed floor assembly, FastFloor, that utilizes conventional W-section beams with a floor plate fastened to the top flanges to form a stable all-steel modular floor unit. A separate raised access floor system is added on top of the floor plate to accommodate services. The floor plate provides lateral restraint to the top flanges of the W-sections, thus the traditional lateral torsional buckling stability mode becomes constrained axis flexural torsional buckling. Additionally, the plate contributes to and changes the vibration frequencies of the W-section beams which together form the assembly. Floor configurations investigated include: a single module that is 10 ft x 40 ft and a full-bay module that is 30 ft x 40 ft. Alternative structural detailing – such as the inclusion of angle blocking and plate stiffeners are considered to further stabilize the assembly, improve the modal frequencies, and potentially improve the accelerations experienced from human walking. Two types of analysis to study vibration are performed in ABAQUS: (1) free vibration analysis for the eigen frequencies and mode shapes, and (2) dynamic analysis simulating footfalls from human walking to find resulting peak accelerations. This study is part of a larger effort in which experimental walking tests were also performed on both the modules.

1. Introduction

The vibration assessment of floor systems requires understanding the eigen frequencies, mode shapes and dynamic response – particularly the peak accelerations that are expected from

[1] Graduate Research Assistant, Johns Hopkins University, <rchidam3@jhu.edu>
[2] Graduate Research Assistant, West Virginia University, <sr00090@mix.wvu.edu>
[3] Graduate Research Assistant, Virginia Polytechnic Institute and State University, <abdelrhman@vt.edu>
[4] Assistant Professor, West Virginia University, <onur.avci@mail.wvu.edu>
[5] Montague-Betts Professor of Structural Steel Design, Virginia Polytechnic Institute and State University, <meather@vt.edu>
[6] Willard and Lillian Hackerman Professor of Civil and Systems Engineering, Johns Hopkins University, <schafer@jhu.edu>

human-induced vibrations. The focus of work here is computational vibration assessment on the new FastFloor prototypes. For commercial construction FastFloor module prototypes consist of 40 ft long W-section beams spaced 5 ft apart and topped with structural plate. To date, both single module (10 ft x 40 ft) and full-bay (30 ft x 40 ft) floors have been experimentally studied (see Rifai, 2025), with and without a raised access floor (RAF) system on the floor plate, and under various bracing details. Here, shell finite element models are developed in ABAQUS and are used to analyze different configurations of FastFloor and assess them for vibration serviceability. These models are intended to expand the experimental work and explore further improvements to the FastFloor system to achieve better vibration performance. This paper provides a brief summary of vibration experiments performed by the larger team and then discusses characterization of the RAF modules through small-scale experiments conducted by the first author. Modeling details for the ABAQUS FastFloor models are then explained, followed by the vibration analyses performed in this study. The benchmark walking experiments of Rifai, 2025a and Rifai, 2025b are simulated. The mode shapes, frequencies and peak accelerations of the studied FastFloor modules are provided and compared against the experimental results.

2. Vibration acceptability criteria for human comfort

AISC Design Guide 11 (AISC DG-11, 2016) provides guidelines on vibrations of steel-framed structural systems due to human activity. Chapter 2 of DG-11 provides the evaluation criteria for human comfort for low frequency floors (fundamental frequency less than 9 Hz) and high frequency floor (fundamental frequency greater than 9 Hz) systems. Fig. 1 shows the recommended tolerance limits for peak acceleration required by DG-11. The FastFloor system is intended for commercial use and the different FastFloor configurations studied have fundamental frequencies falling in the range of 7 Hz to 12 Hz. Hence, for the system to be acceptable the equivalent sinusoidal peak accelerations should be no more than 0.5 %g – 0.7 %g.

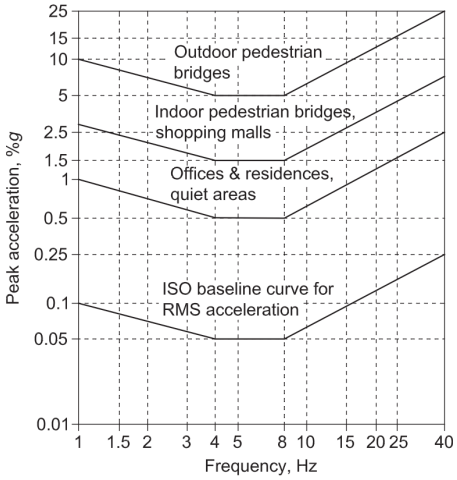

Figure 1: Recommended tolerance limits for human comfort (AISC DG-11, 2016)

3. Vibration Testing

Vibration experiments were performed on a single module 10 ft x 40 ft (Fig. 2a) and full-bay 30 ft x 40 ft modules (Fig. 2b) to find the frequencies, mode shapes, damping and acceleration response by the larger team. These experiments are used for benchmarking in this study. Details of experiments, procedures and observations can be found in papers – Rifai (2025a,b,c) and the summary of Schafer (2024). The experiments involved low amplitude shaker excitations to find

the vibration frequencies, mode shapes and the corresponding damping ratio for each frequency. Active vibration modes in the range of 1 – 30 Hz were considered. Random and synchronous walking tests were performed, and acceleration time-histories were obtained. Fig. 2 shows walking tests on both the single module and full-bay modules after the raised access floor (RAF) was added. The tests considered different options for supporting the beams and plate and for the full-bay tests options to add superimposed dead load and supplemental damping such as adding sandbags and additional people standing on the floor.

(a) (b)

Figure 2: Experimental walking tests on (a) single module with RAF
(b) full-bay module with RAF (Rifai, 2025b)

4. Experimental characterization of Tate ConCore 1000 RAF module

A feature of the FastFloor system is the utilization of a Raised Access Floor (RAF). Unlike the W-section beams and plates, from a vibration standpoint the RAF modules are a relatively complicated collection of tubes, connectors, and formed floor parts. As a result, it was decided that small-scale tests of the RAF may be useful for inclusion in the full floor module models. These tests were conducted by the first author and described herein. The RAF is made up of repeating modules consisting of a panel on 4 pedestals as shown in Fig. 3. A series of vibration tests are performed on the RAF unit where the acceleration response under free vibration is recorded. The time history results from the experiments are processed further to obtain the fundamental vibration frequencies that can be used to find simplified properties for modeling.

4.1. Test procedure

The RAF module was tested under two conditions: (1) fixed to a heavy optical table using bolts, and (2) fixed to a concrete floor using Seal bond 95 adhesive - as used in field installations. Accelerometers were positioned vertically and horizontally as shown in Fig. 3a and Fig. 3b respectively. An impact hammer was used to apply an impact load on the RAF plate to create free vibrations on the RAF set up. Four accelerometers were used in the vertical direction to obtain the vertical flexural mode, and one accelerometer was used in the horizontal direction to obtain the horizontal sway mode for the RAF set up. Acceleration time-histories were recorded using LabView software that was further processed to find the fundamental frequencies.

(a) (b)

Figure 3: Experimental setup of the RAF module with accelerometers (a) RAF module fixed to the optical table using bolts (b) RAF module fixed to the floor using seal bond 95 adhesive

4.2. Vibration frequencies

Acceleration time-history results from LabView were processed in MATLAB using a fast Fourier transform (FFT) to find the fundamental frequencies for the vertical and horizontal modes. The resulting FFTs are shown in Fig. 4a and Fig. 4b.

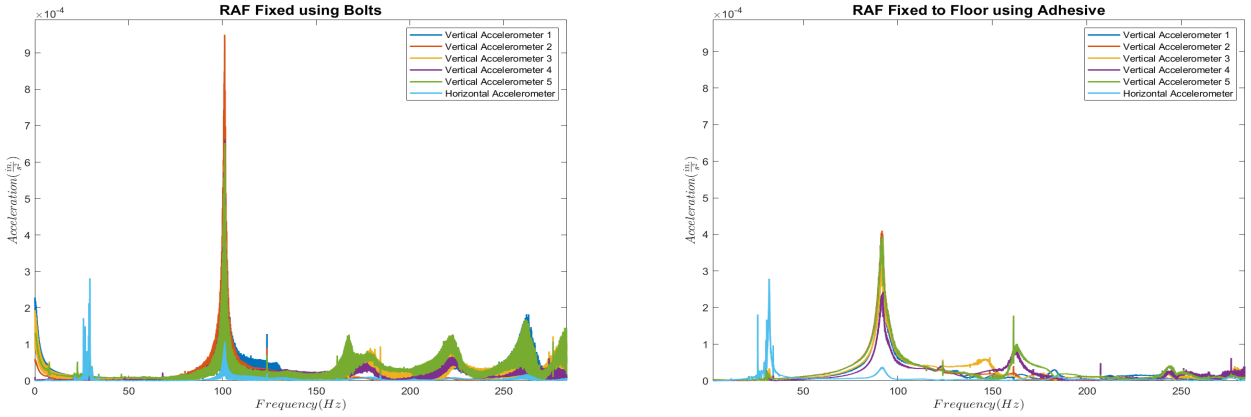

(a) (b)

Figure 4: FFTs for (a) RAF module fixed to the optical table using bolts (b) RAF module fixed to the floor using seal bond 95 adhesive

The fundamental vibration frequency for the flexural mode was found to be 100 Hz and that of the sway mode was found to be 25 Hz.

4.3. Converting frequencies to model inputs

A finite element model appropriate for inclusion in our larger FastFloor assembly model, consisting of the small bottom RAF base plates (shell elements S4R), pedestal tubes (beam elements B31), and top RAF panel (shell elements S4R) is developed. S4R is a 4-noded thin plate quadrilateral element that uses linear interpolation and can be used to capture large strains in shells, and B31 is a first-order beam element (See ABAQUS, 2024). The top RAF panel is modeled as a flat plate; however, the density and thickness of this equivalent RAF panel must be determined. In reality, the RAF panel is thicker at the center and thinner towards the edges and the panel has corrugations with void spaces. Eq. 4.3-1 through 4.3-3 are used to derive a simplified value for

density and uniform thickness that can be used for the RAF panel in the model. The vibration frequencies from the experiments described in Section 4.2 are used in the equations below, while keeping the properties of the RAF such as the mass and area to be constant, to obtain the equivalent fat plate thickness, density, and Young's modulus.

$$k = \omega^2 m \tag{4.3-1}$$

$$D = \frac{Et^3}{12(1-\nu^2)} \tag{4.3-2}$$

$$\rho = \frac{m}{At} \tag{4.3-3}$$

where,

k = Stiffness, $kip/in.$
ω = Circular vibration frequency, rad/s
m = Mass of the RAF, $kip - s^2/in.$
D = Flexural rigidity, $kip - in.$
E = Young's modulus, ksi
t = Thickness, $in.$
ν = Poisson's ratio = 0.3
ρ = Density of the RAF panel, $kip - s^2/in.^4$
A = Area of the RAF panel, $in.^2$

Mass of the RAF is obtained as,

$$m = \frac{Measured\ weight\ of\ the\ RAF\ panel}{Acceleration\ due\ to\ gravity}$$

$$m = \frac{0.00299\ kip}{386\ in./s^2} = 7.77 * 10^{-5}\ kip - s^2/in.$$

Area of the RAF panel is,

$$A = (24\ in.)^2 = 576\ in.^2$$

Young's modulus of the RAF panel is assumed to be that of concrete,

$$E = 4000\ ksi$$

The thickness of the RAF panel varies from a minimum of 0.1 in. at the edges to 1.65 in. at the center. After several iterations, using the thickness of 1 in. in Eq. 4.3-1 through 4.3-3 we have,

$$t = 1\ in.$$

$$D = \frac{4000\ ksi * (1\ in.)^3}{12(1-0.3^2)} = 366.3\ kip - in.$$

$$\rho = \frac{(7.77 * 10^{-5}\ kip - s^2/in.)}{576\ in.^2 * 1\ in.} = 1.35 * 10^{-7}\ kip - \frac{s^2}{in.^4}$$

Using the derived thickness, density and Young's modulus from above as inputs to the model and performing a free vibration analysis results in the vibration modes shown in Fig. 5 and Fig. 6.

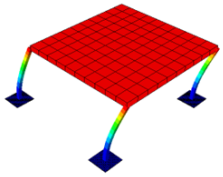

Figure 5: ABAQUS Horizontal Sway Mode 25 Hz

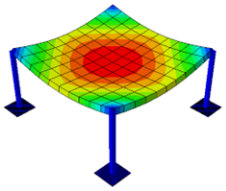

Figure 6: ABAQUS Vertical Flexure Mode 100 Hz

In the equivalent flat plate RAF model the sway mode frequency is 25 Hz, and the plate flexural mode frequency is 100 Hz, matching the experimental results. Having verified the model vibration frequencies and mode shapes using simplified properties, this model can now be used for the RAF in the larger assembly as described in the following sections.

5. Finite element modeling and analysis

Finite element models of the FastFloor prototypes are created and analyzed to examine the vibration serviceability of each of the configurations studied.

5.1. FastFloor naming convention

Table 1 provides the list of FastFloor configurations analyzed in this study. Starting with the baseline module, additional structural detailing such as angle blocking and plate stiffeners is included to examine its effects on the vibration performance.

Table 1: Selected FastFloor Modules

Nomenclature	**Details**
Single Module (SM)	
SM94 Bare	Three W24x94 beams with web stiffeners and ½ in. floor plate
SM94 RAF	Three W24x94 beams with web stiffeners and ½ in. floor plate topped with RAF
SM94 RAF AB L/3	Three W24x94 beams with web stiffeners and ½ in. floor plate topped with RAF and L3x3x1/4 angle blocking at third points
SM94 RAF PS+AB L/3	Three W24x94 beams with web stiffeners and ½ in. floor plate topped with RAF and L3x3x1/4 angle blocking at third points and L3x3x1/4 plate stiffeners at third points
Full Bay (FB)	
FB68 RAF AB1356	Seven W24x68 beams and ½ in. floor plate topped with RAF and L3x3x1/4 angle blocking at third points in bays 1,3,5,6

5.2. Modeling details

Shell finite element models are created for all the FastFloor configurations listed in Table 1. For the baseline module, i.e., no RAF added, all the components are modeled using shell S4R elements (See ABAQUS, 2024) which is a 4-noded thin plate quadrilateral element that uses linear interpolation and can be used to capture large strains in shells. When RAF is in place, the RAF module components are modeled as described in Section 4.3.

Fig. 7 shows an assembled 10 ft x 40 ft SM94 Bare model which consists of three W24x94 beams 42 ft long (out-to-out) with beams spaced at 5 ft from each other and a 1/2 in. floor plate 40 ft long that is connected to the top flanges using multi point constraints at the locations of bolts or welds. (In this specimen the plate is stitch welded to the first two beams and bolted to the third (outer) beam – see Rifai, 2025b for details). Web stiffeners ¾" thick are attached to the beams at the ends. Other variations such as the inclusion of angle blocking and plate stiffeners are modeled by adding to the baseline module.

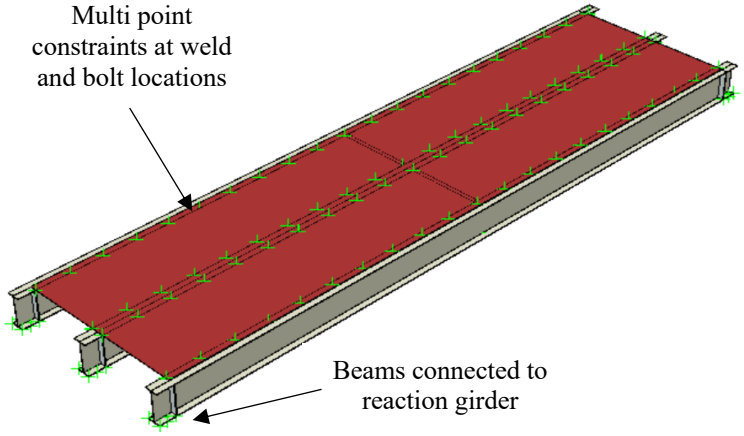

Figure 7: Assembled SM94 Bare module in ABAQUS

Fig. 8 shows an assembled and meshed 10 ft x 40 ft SM94 RAF which consists of the baseline module and RAF modules with 2 ft x 2 ft panels defined with a uniform thickness of 1 in. (as explained in Section 4), pedestals 0.9 in. x 0.9 in. and base plates 4 in. x 4 in..

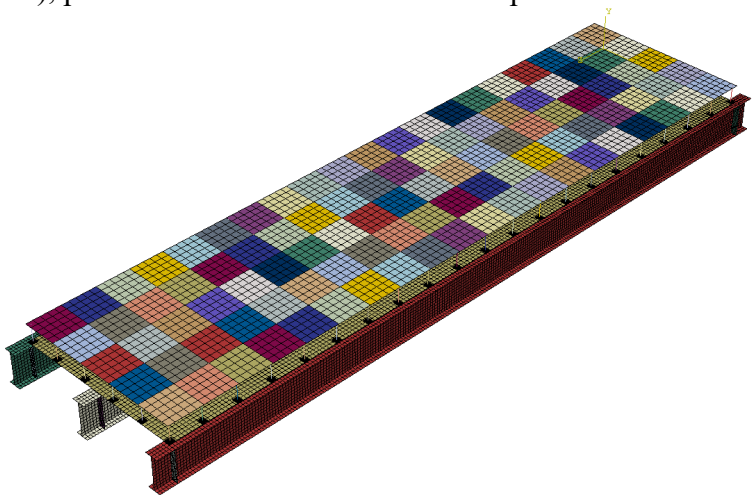

Figure 8: Meshed SM94 RAF module in ABAQUS

Fig. 9 shows an assembled full-bay (30 ft x 40 ft) model which consists of ½" floor plates with W24x68 beams. It's important to note that unlike the single module, these full-bay models also have girders (two W30x108) and columns (four W14x398) included in the model. The assembly also includes angle blocking in bays 1,3,5, and 6 as indicated in Fig. 10.

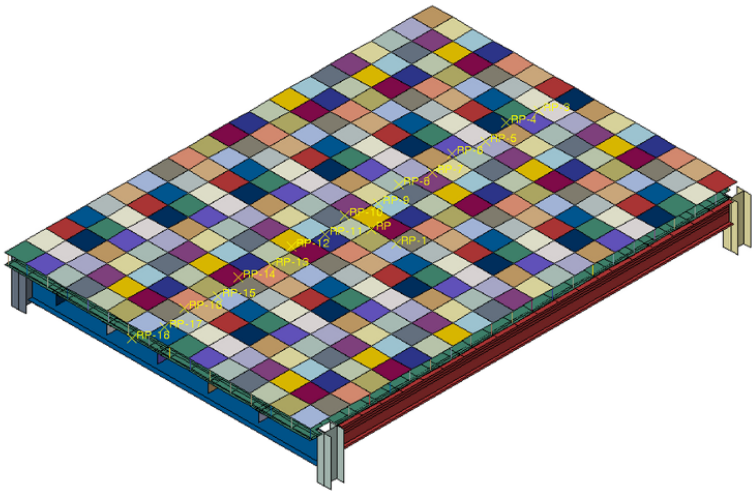

Figure 9: Assembled 30'x40' full-bay module with angle blocking (FB68 AB 1356) in ABAQUS

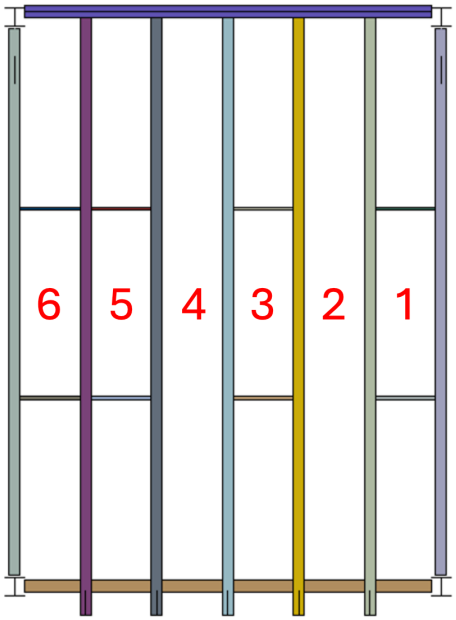

Figure 10: Plan view showing bays in a full-bay module,
including angle blocking in bays 1,3,5, and 6

Material properties for all the components except for the RAF panel are defined as steel with $E = 29000$ ksi, $\nu = 0.3$, and $\rho = 7.5 * 10^{-7}\ kip - s^2/in.^4$ and for the RAF panel plate $E = 4000$ ksi, $\nu = 0.3$, and $\rho = 1.35 * 10^{-7}\ kip - s^2/in.^4$ is used as derived in Section 4. All the components are connected by defining multi point tie constraints at the necessary locations that correspond to bolts, welds and adhesives used in experimentally tested models. Multi point constraints tie the defined node sets and the degrees of freedom of a secondary set with that of a

primary set – the modeler decides which degrees of freedom (DOF) are tied. Table 2 lists the connection between components, the primary set and the secondary set, and the DOF tied.

Table 2: Interaction between components in model

Components connected	Primary set	Secondary set	DOF tied
Beam to web stiffeners	Beam	Web stiffeners	Translations and rotations
Beams to floor plate	Beams	Floor plate	Translations
Floor plate to base plates	Floor plate	Base plates	Translations
Base plate to pedestal	Base plate	Pedestal's bottom node	Translations and rotations
Pedestal to RAF panel	Pedestal's top nodes	RAF panel	Translations

Bearing boundary conditions are simulated in the single module models by selecting the nodes at the beam ends that correspond to the locations were the support girders (which were themselves directly resting on the floor) were present. For full-bay models, the nodes at the base of the four columns are fixed, similar to the test setup.

5.3. Best fit damping

During the experiments summarized in Rifai (2025a,b) a modal testing using low amplitude shaker excitations were used to obtain vibration frequency, mode shape and damping ratio for each of the modes. For models used in this study Rayleigh damping is used which allows for defining damping coefficients a and b for a damping ratio β shown in Eq. 5.3-1 and Eq. 5.3-2 (Chopra, 2007).

$$a = \beta \frac{2\omega_1 \omega_2}{\omega_1 + \omega_2} \tag{5.3-1}$$

$$b = \beta \frac{2}{\omega_1 + \omega_2} \tag{5.3-2}$$

where,

a = Mass- proportional damping coefficient, s^{-1}
b = Stiffness-proportional damping coefficient, s
ω_1, ω_2 = Circular vibration frequencies, rad/s
β = Damping ratio

Damping ratio β for each model configuration is selected based on a best fit method implemented in MATLAB. The resulting damping ratio is compared with the known experimental damping ratios across corresponding frequencies and iterated for the best set of β and ω's until the sum of square of errors between the two are minimal over a selected frequency range. For example, the measured experimental damping from modal testing for SM94 Bare is shown in Fig. 11. The range of damping ratios for this case was found to be 0.1% to 0.4% across the modes considered up to 30 Hz. A best fit $\beta = 0.26\%$ at $\omega_1 = 61.2\ rad/s$ ($f_1 = 9.7\ Hz$) and $\omega_2 = 153.2\ rad/s$ ($f_2 = 24.4\ Hz$) was found as shown in Fig. 12.

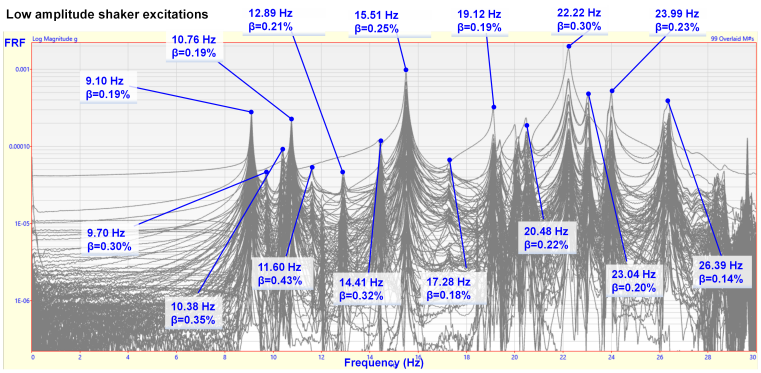

Figure 11: Example measured experimental damping for SM94 Bare from modal testing in Rifai (2025a)

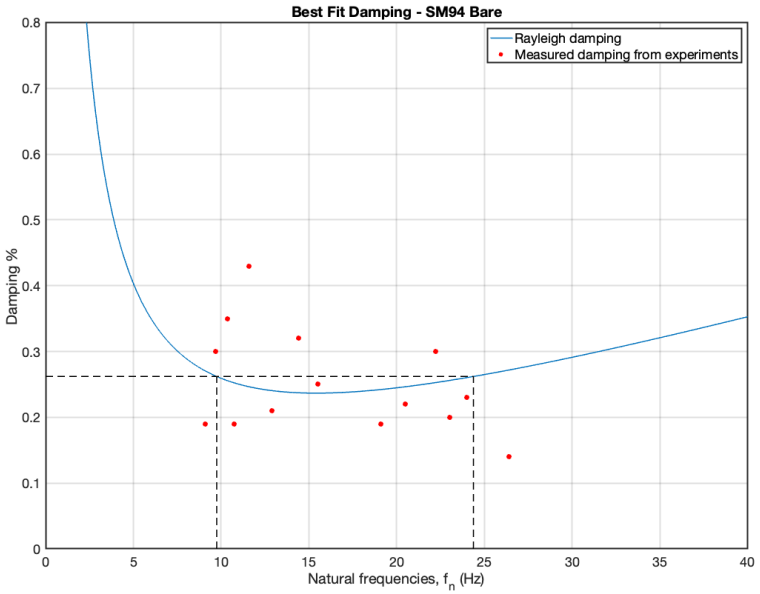

Figure 12: Best fit damping curve for SM94 Bare model

Table 3 summarizes the experimental damping ratios and the best fit Rayleigh damping ratios for all the single module models that are utilized in the walking simulations.

Table 3: Experimental and best fit damping ratios

FastFloor Configuration	Experimental Damping Ratio (%)	Best Fit Damping Ratio (%)	ω_1 (rad/s)	ω_2 (rad/s)
SM94 Bare	0.2% - 0.4%	0.26%	61.2	153.2
SM94 RAF	0.6% - 0.9%	0.72%	68.2	147.0
SM94 RAF AB L/3	0.3% - 1.0%	0.70%	70.8	169.3
SM94 RAF PS+AB L/3	0.3% - 1.0%	0.65%	71.2	146.1

5.4. Free vibration analysis

Free vibration analysis is performed on the model to extract the eigen frequencies and vibration mode shapes. Vibration mode shapes are compared with experimental mode shapes to ensure that similar modes are compared. Note, the experiments used a dense set of accelerometers to precisely capture modes that deform in the vertical direction and the visualization of the modes thus only

provides the vertically observed motion; however, the model includes and provides visualization for all deformations including beam constrained axis flexural torsional modes which include significant horizontal motion and are prominent in some cases as detailed, for example, in the results of Section 6.1.

5.5. Walking simulations

Simulations are also performed to examine the floor module response to human-induced motion through walking. The simulations are motivated from the benchmark experiments of Rifai et al. (2025a,b,c). The key output from the tests and simulations is the acceleration time-histories experience from a fixed location as another person walks the floor. Since the module is more sensitive to some walking frequencies than others, care must be taken both in the experiments and simulations. For the model, we explicitly input time series of footfalls at a specified walker frequency – a subharmonic of the system's natural frequency that falls in typical walking frequency range is used for "synchronous walking" and a constant frequency of 1.5 Hz is used to compare against "asynchronous" or "random walking" in experiments. A typical range of walking frequency from 90 to 120 BPM (1.5 to 2 Hz) is assumed.

Walking creates a complex force-time relationship; however, Cai (2019) studied a variety of models and recommended a specific model employed here. For an average human weight of 157 lb (as recommended in AISC DG-11) each foot strike (left, right, etc.) is applied as load varying with time and location in the dynamic analysis, following Eq. 5.5-1 as illustrated in Fig. 13.

$$F(t) = 157(K_1 t + K_2 t^2 + K_3 t^3 + K_4 t^4 + K_5 t^5 + K_6 t^6 + K_7 t^7 + K_8 t^8) \qquad (5.5\text{-}1)$$

The coefficients, K_i's, are determined as a function of walker frequency (Cai, 2019). It is important to note that walkers are included only through forcing function $F(t)$ – mass and in particular damping of walker's are not modeled (and known to have some impact). Further the walker does not react, or change based on the floor response – which is also known to occur.

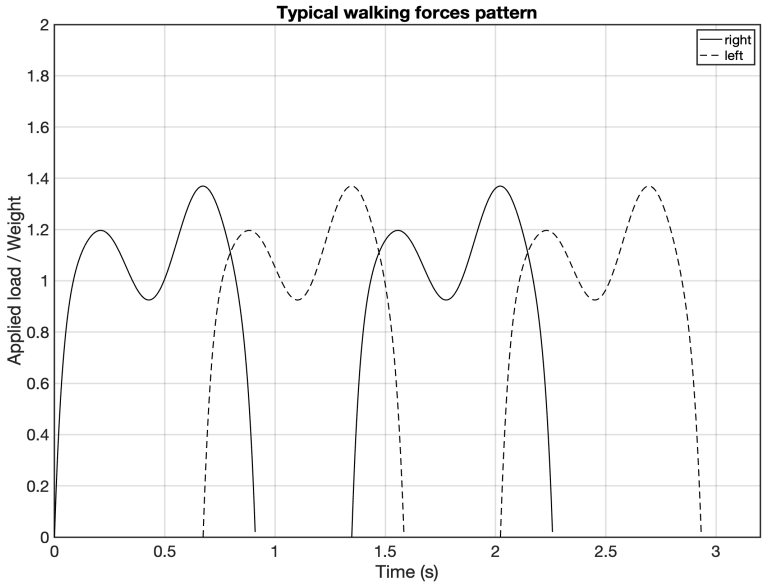

Figure 13: Force-time relationship for footfalls from typical walking (Cai, 2019)

Walking forces $F(t)$ at the footfall locations are defined as amplitudes in the model and the dynamic implicit analysis provides acceleration time-history response. For the single module models the walking is simulated in the mid length of one of the bays (red line) and the response is measured at the midpoint of the adjacent bay (red dot) as shown in Fig. 14. Similarly, for the full-bay models walking is modeled at the mid length of bay 4 and the response is measured at the midpoint of bay 3 as shown in Fig. 15. These locations are consistent with experiments and are assumed to be the worst possible locations for experiencing walking-induced accelerations.

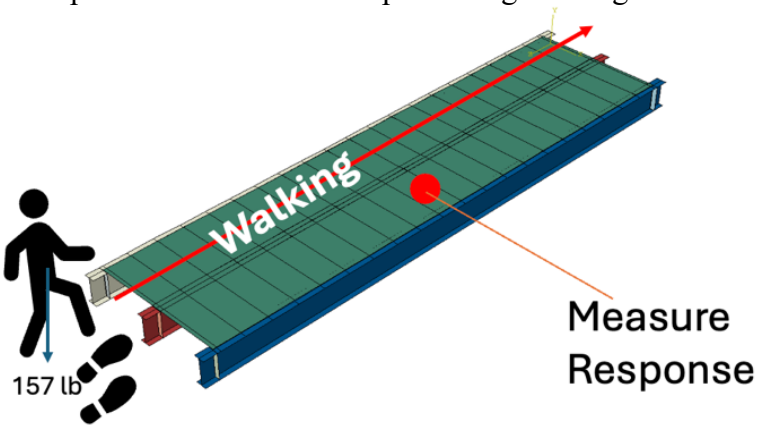

Figure 14: Walking on SM68 Bare in ABAQUS

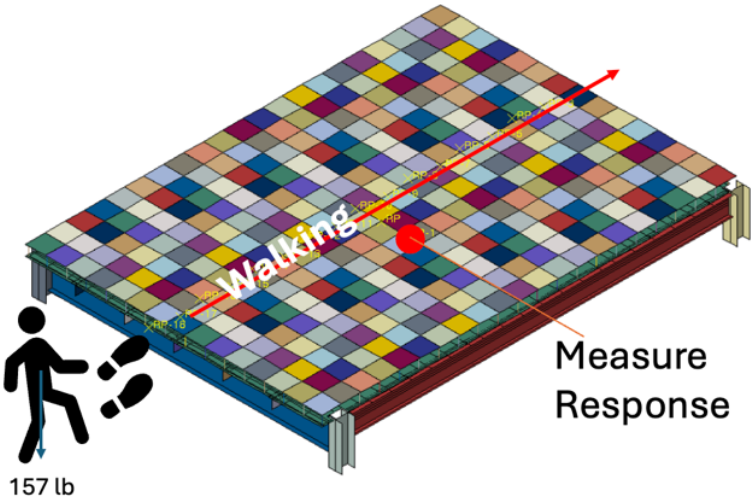

Figure 15: Walking on FB68 RAF AB1356 in ABAQUS

An example of the full-bay acceleration time history output from the model for the FB68 RAF AB1356 from synchronous walking at 111 BPM (1.85 Hz) corresponding to the 4th harmonic of the fundamental frequency (7.4 Hz / 4 = 1.85 Hz) and a damping ratio of $\beta = 2.25\%$ is provided in Fig. 16. The raw time-history signals are processed: (1) the measured response is filtered using a frequency weighted procedure as per SCI British standards (Smith, 2009), (2) the maximum equivalent sinusoidal peak acceleration (ESPA) is found per AISC-DG11, which itself involves finding the peak of the 1-second root mean square (RMS) of the frequency weighted response multiplied by $\sqrt{2}$ (AISC DG-11, 2016). In addition, an FFT of the measured response for FB68 RAF AB 1356 from the model is also shown in Fig. 17. The peaks of the FFT correspond to subharmonics of the natural frequencies of the module.

6. Results

This section presents the eigen frequencies and mode shapes resulting from the free vibration analysis of the shell finite element model compared with the benchmark experiments. These results are shown for single module and full-bay variants of FastFloor described in Section 5.1. Acceleration time-histories, ESPAs and their corresponding FFTs resulting from walking simulations are also provided.

6.1. Mode shapes and frequencies

Tables 4 and 5 provide the frequencies, mode shapes and a description for each mode from the experiments and the model. The results are shown for the first three modes for the single module and full-bay models. The experimental mode shapes display the plate deformation in the vertical direction since the results were recorded with accelerometers positioned at the top surface (floor plate or RAF plates depending on the model). The model mode shapes display the deformation of the whole system including the beams for the single module models and beams, columns and girders for the full-bay models.

Table 4: Mode shapes and frequencies for SM94 without RAF

Configuration	Mode	Experiment		Model		Comments
		f_n (Hz)	Mode Shape	f_n (Hz)	Mode Shape	
SM94 Bare	1	9.10	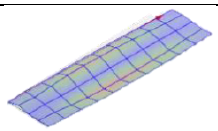	9.7	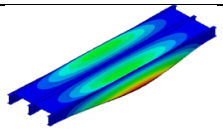	Beams in CAFTB out-of-phase
	2	10.76	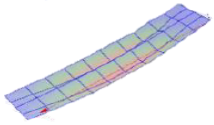	11.9	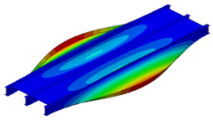	Outer beams in CAFTB out-of-phase and center beam in flexure
	3	12.89	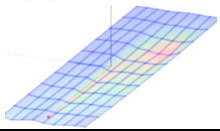	13.1	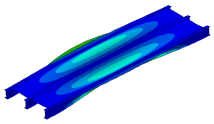	All beams in CAFTB in-phase

Table 5: Mode shapes and frequencies for SM94 with RAF

Configuration	Mode	Experiment		Model		Comments
		f_n (Hz)	Mode Shape	f_n (Hz)	Mode Shape	
SM94 RAF	1	9.2	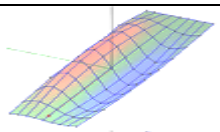	10.8	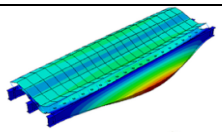	Beams in CAFTB out-of-phase. Second plate mode
	2	10.3	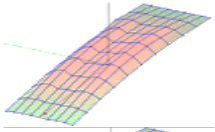	12.5	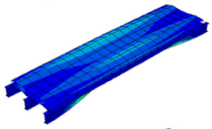	Outer beams in CAFTB out-of-phase and center beam in flexure
	3	13.7	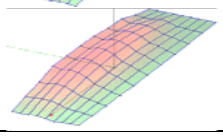	13.6	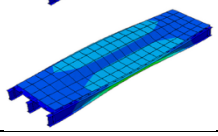	All beams in CAFTB in-phase. RAF plates in a combination of swaying and flexure

SM94 RAF AB L/3	1	9.5	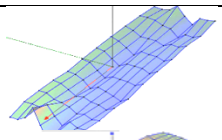	11.3	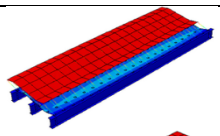	Beams in CAFTB in-phase
	2	10.8	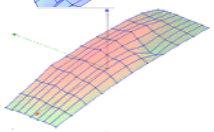	11.5	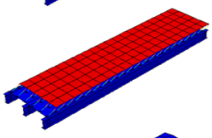	RAF plates in a combination of swaying and flexure
	3	11.8	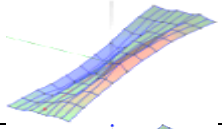	13.5	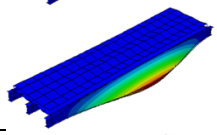	Beams in CAFTB in-phase
SM94 RAF PS+AB L/3	1	10.5	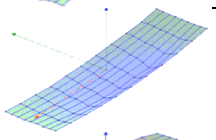	11.4	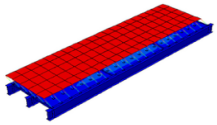	Beams in CAFTB in-phase
	2	11.7	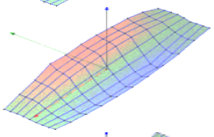	11.6	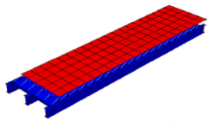	RAF plates in a combination of swaying and flexure
	3	12.7	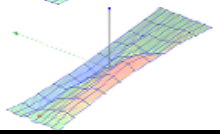	13.8	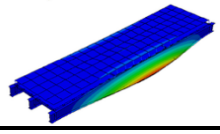	Beams in CAFTB in-phase

Table 6: Mode shapes and frequencies for FB68 RAF AB 1356

Configuration	Mode	Experiment		ABAQUS		Comments
		f_n (Hz)	Mode Shape	f_n (Hz)	Mode Shape	
FB68 RAF AB 1356	1	7.37	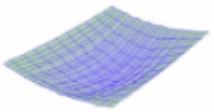	7.42	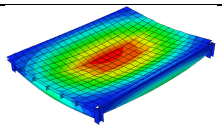	Beams in flexure
	2	9.57	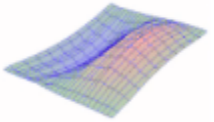	9.66	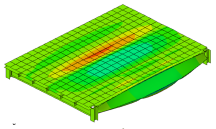	Beam pairs in CAFTB and twisting in-phase and out-of-phase
	3	11	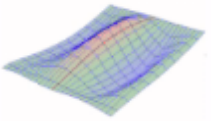	10.74	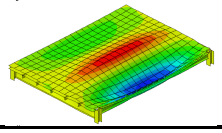	Beams pairs in flexure and CAFTB

6.2. Equivalent sinusoidal peak accelerations

Acceleration time-histories were processed to obtain ESPAs through the procedure described in Section 5.5. The results for the single module models from the walking simulations in comparison to the experimental walking tests are summarized in Table 7.

Table 7: ESPAs from experiments and walking simulations on single module models

FastFloor Model	Experiment			Walking Simulation	
	Damping ratio (%)[1,2,3]	Min-Max ESPA (%g)[4,5]	Mean ESPA (%g)	Best Fit Damping Ratio (%)[6]	ESPA (%g)
SM94 Bare	0.2 – 0.4	0.1 – 3.1	0.8	0.26	1.2
SM94 RAF	0.6 – 0.9	0.3 – 1.8	0.6	0.72	0.88
SM94 RAF AB L/3	0.3 – 1.0	R 0.2 – 0.5 S 0.5 – 1.4	R 0.4 S 0.8	0.7	R 0.75 S 0.81
SM94 RAF PS+AB L/3	0.3 – 1.0	R 0.2 – 0.5 S 0.3 – 1.2	R 0.4 S 0.7	0.65	R 0.64 S 1.00

R = Random walker frequency in the experiments and step frequency of 1.5 Hz in models; S = Synchronous walking at one of the subharmonics of the fundamental eigen frequency that falls in the range of walking 1.3 Hz to 2 Hz
1–Obtained by using low-amplitude shaker excitation tests
2 – Modal damping ratios are amplitude-dependent. Each mode has a different damping ratio. Damping ratios were determined in frequency domain per FRFs
3 – Low-amplitude shaker tests were considered which correspond to walking excitation amplitudes (rather than high-amplitude shaker tests)
4 – ESPA: Equivalent Sinusoidal Peak Acceleration. Determined based on walking with subharmonics of modal frequencies guided with metronome
5 – Calculated per AISC DG-11, Chapter 7 procedures. The method provides estimations for peak walking accelerations to be compared with recommended limits.
6 – Damping was pre-defined in models using Rayleigh damping method

Acceleration time-history output and FFT of the full-bay model: FB68 RAF AB 1356 for a damping ratio of 2.25% from walking simulation are shown in Fig. 16 and Fig. 17. ESPAs for the FB68 RAF AB 1356 across varying damping ratios from the experiments and walking simulations are compared in Table 8. The results correspond to synchronous walking at around 111 BPM, and this walker step frequency was chosen so it falls in the usual walking range of 90 – 120 BPM while achieving the subharmonics of the system frequency. A dead load of 12 psf was added on the RAF in the experiments. This was accounted for in the walking simulations by increasing the density of the RAF material from 1.35×10^{-7} kip $- s^2/in.^4$ to 3.51×10^{-7}kip $- s^2/in.^4$.

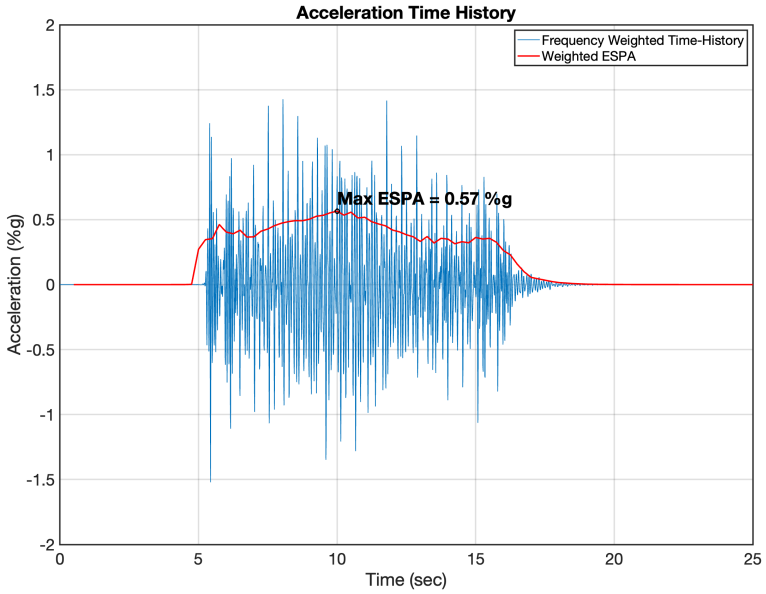

Figure 16: Acceleration time-history for FB68 RAF AB1356 under synchronous walking ($\beta = 2.25\%$) from walking simulation

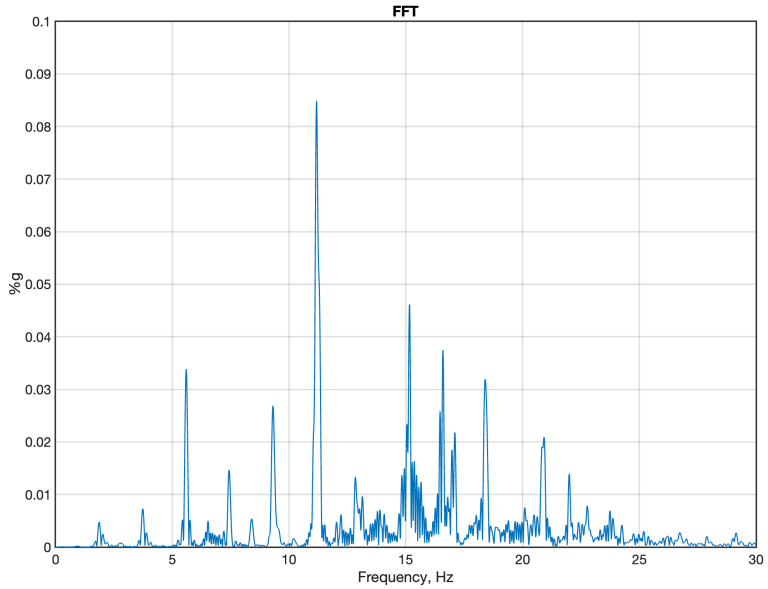

Figure 17: Fast Fourier Transform for FB68 RAF AB1356 under synchronous walking ($\beta = 2.25\%$) from walking simulation

Table 8: ESPAs from experiments and ABAQUS walking simulations on FB68 RAF AB 1356

Damping Ratio (%)	Experiment	Walking Simulation
	ESPA (%g)	ESPA (%g)
0.5	1.20	1.93
1	0.84	1.04
1.5	0.69	0.73
2.25	0.57	0.51
3	0.50	0.39
3.5	0.48	0.34
4	0.44	0.30

Under the studied remediations (angle blocking, AB and plate stiffeners, PS) Fig. 18 compares the FFTs of the SM94 models. The acceleration time-history outputs are used to create these FFTs, as described in Section 5.5. A constant walker step frequency of 1.5 Hz is utilized across the models reported in Fig. 18.

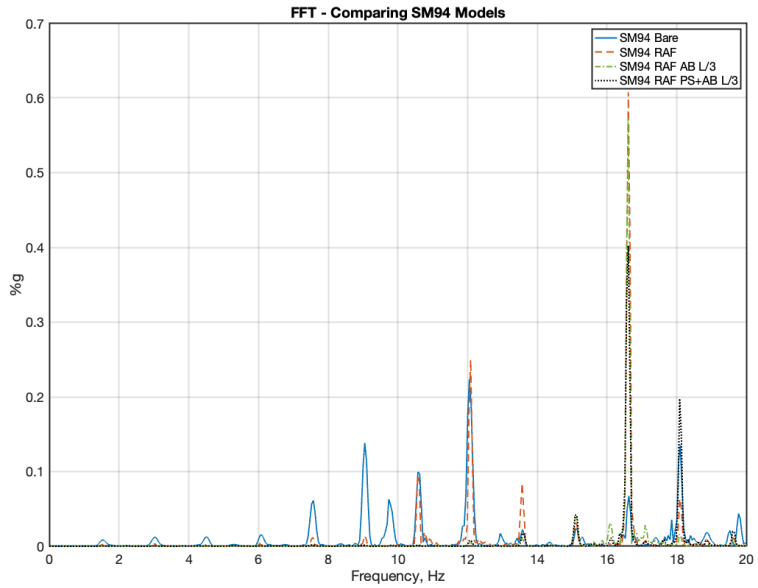

Figure 18: Comparing FFTs of different SM94 models from walking simulations

Assuming synchronous walking at 111 BPM Fig. 19 provides a comparison between the experimental and walking simulation ESPAs across various damping ratios for the full-bay FB68 RAF AB1356. In the experiments, damping was varied by the addition of sandbags and additional people standing still on the floor. In the models, damping was varied through β in the Rayleigh damping expression.

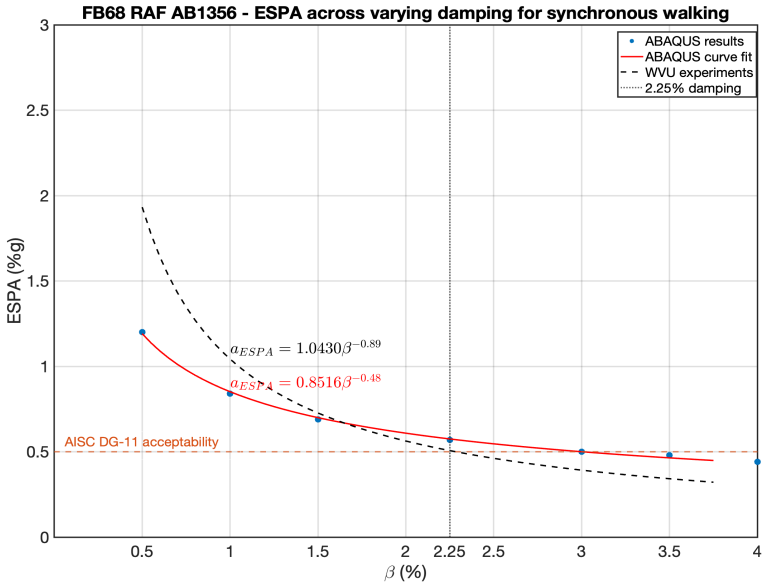

Figure 19: Comparing experimental vs model ESPAs across varying damping for FB68 RAF AB1356

7. Discussion

The results demonstrate that the shell finite element models can reasonably predict vibration frequencies and mode shapes for the floor module studied. In addition, since the model provides output at all locations – features such as twisting in the beams are highlighted that are not as obvious in experiments focused on vertical accelerations. The results also show that explicit

walking simulations can be utilized to predict ESPA for consideration of vibration acceptance. However, differences in ESPAs between experiments and the models are not always small and further improvements are possible. The ESPA results for both experiments and models are sensitive to the processing methods employed – and sensitivity study to this step would be warranted. The experimental damping ratios are both frequency and amplitude dependent, both effects of which are simplified in the current model. The use of humans on the floor to increase damping is like adding point-based fluid dampers – while in the model whole model damping is implemented. The step frequency in experiments is aided by an audible metronome; however, in the model step frequency is perfect, leading to variation between the two – and the reality that the model can match subharmonics exactly leading to maximum amplifications, but this is unlikely in the lab. The model and experiments are not in perfect agreement, but the overall magnitudes are similar, as are the trends, and given the complexity it is asserted that the model can provide meaningfully accurate ESPA predictions for further studies. Again, sensitivity studies could potentially provide further insight. Considering the results more broadly, Fig. 19 demonstrates that the full-bay floor configuration provides acceptable accelerations at a damping ratio around $\beta = 2.25\%$, since the ESPA is less than 0.5%g. Overall, adding the RAF to the system modestly improves damping and decreases ESPA, and moving to the full-bay configuration from the single module also reduces ESPA.

8. Conclusions

This study investigated the vibration performance of different FastFloor configurations using high fidelity shell finite element models and validated the results using benchmark experimental results. Reliable results were achieved through the proposed method for walking simulations and the simulations reasonably matched with experiments, especially for the full-bay models. Currently, damping ratio measured from experiments is being provided as input to the models. Work is underway to further improve the finite element models by exploring frequency dependent and amplitude dependent damping options to bring the results even closer to the experiments. Hence, it can be concluded that it is now possible to utilize walking simulations to gain more insights on impact of structural detailing on floor vibrations and can be used to predict expected floor accelerations in the studied module.

Acknowledgments

This research was sponsored by the Charles F. Pankow Foundation, American Institute of Steel Construction (AISC), MKA Foundation, and Johns Hopkins University. This work is being conducted in coordination with the AISC “Need for Speed” initiative under the auspices of the Steel Diaphragm Innovation Initiative. Any findings, conclusions or recommendations expressed in this paper are those of the authors and do not necessarily reflect the views of any sponsors.

References

Dassault Systèmes Simulia Corp. (2016). ABAQUS Analysis User’s Manual, Version 6.6. Providence, RI. Accessed Feb. 26, 2024. Available online: https://classes.engineering.wustl.edu/2009/spring/mase5513/abaqus/docs/v6.6/books/usb/default.htm

American Institute of Steel Construction (AISC). (n.d.). Design Guide 11: Vibrations of Steel-Framed Structural Systems Due to Human Activity, 2nd ed. Chicago, IL. Accessed Apr. 16, 2025. Available online: https://www.aisc.org/Design-Guide-11-Vibrations-of-Steel-Framed-Structural-Systems-Due-to-Human-Activity-Second-Ed

Y. Cai, G. Gong, J. Xia, J. He, and J. Hao, “Simulations of human-induced floor vibrations considering walking overlap,” SN Applied Sciences, vol. 2, no. 1, p. 19, Jan. 2020, doi: 10.1007/s42452-019-1817-1.

Chopra, A.K. (2007). Dynamics of Structures: Theory and Applications to Earthquake Engineering, 3rd ed. Prentice Hall, Upper Saddle River, NJ. Available online: https://www.pearson.com/en-us/subject-catalog/p/dynamics-of-structures-theory-and-applications-to-earthquake-engineering/P200000003471/9780137602605

Smith, A.L., Hicks, S.J., and Devine, P.J. (2009). Design of Floors for Vibration: A New Approach, rev. ed. Steel Construction Institute, Ascot, U.K., SCI Publication P354. Available online: https://www.steel-sci.com/publications/design-of-floors-for-vibration-p354/

Rifai, S., Chidambaram Muthu Kumar, R., Abla, F., Rababah, A., Avci, O., Eatherton, M.R., and Schafer, B.W. (2025a). "Effect of bottom flange angle blocking on the dynamic response of two all-steel laboratory floors." *Proceedings of the 43rd IMAC, A Conference and Exposition on Structural Dynamics 2025*, River Publishers. doi:10.13052/97887-438-0147-4_3.

Rifai, S., Chidambaram Muthu Kumar, R., Avci, O., Schafer, B.W., Eatherton, M.R., Easterling, W.S., and Hajjar, J.F. (2025b). "Modal testing and finite element model updating of a Fast-Floor specimen: A modular all-steel floor system." *Proceedings of the 43rd IMAC, A Conference and Exposition on Structural Dynamics 2025*, River Publishers. doi:10.13052/97887-438-0147-4_4.

Rifai, S., Abla, F., Rababah, A., Chidambaram Muthu Kumar, R., Schafer, B.W., Eatherton, M.R., and Avci, O. (2025c). "Vibration serviceability evaluation of an all-steel floor system using the high-frequency floor procedure." *Dynamics of Civil Structures, Vol. 2: Proceedings of the 43rd IMAC, A Conference and Exposition on Structural Dynamics 2025*, River Publishers. doi:10.13052/97887-438-0147-4_10.

Schafer, B., Avci, O., Easterling, W.S., Eatherton, M., and Hajjar, J. (2024). "FASTFLOOR – Development of a novel modular steel floor system for commercial construction in the United States." Preprint, Dec. 2. doi: 10.31224/4183.